

Deciphering the Role of Ocean Dynamics in Equatorial Pacific Decadal Variability

Yu Zhang¹, Shi-Yun Yu¹, Shang-Ping Xie², Dillon J. Amaya³, Qihua Peng⁴, Yu Kosaka⁵, Xiaopei Lin⁶, Jun-Chao Yang¹, Sarah M. Larson⁷, Arthur J. Miller⁸, and Lei Fan¹

¹Ocean University of China

²UCSD

³University of Colorado Boulder

⁴SCSIO

⁵University of Tokyo

⁶Physical Oceanography Laboratory, Ocean University of China

⁷North Carolina State University

⁸Scripps Institution of Oceanography

November 24, 2022

Abstract

Equatorial Pacific decadal variability (EPDV) modulates global climate. Although EPDV is suggested to be generated by both air-sea thermodynamically coupled slab ocean models (SOM) and fully coupled dynamic ocean models (DOM), the reason of EPDV simulated by the two distinct hierarchies of models remains unclear. This ambiguity arises from a gap in the dynamical framework between SOM and DOM. To fill the gap, we conducted a novel experiment (Clim-tau) that retains only the effects of thermodynamic coupling and mean ocean current on EPDV (without anomalous ocean current). We showed that in Clim-tau, thermodynamic-driven EPDV as in SOM is largely damped by equatorial Pacific mean upwelling; whereas involving anomalous ocean current as in DOM, the damped EPDV will be further amplified. Finally, we discussed the role of ocean dynamics in the observed EPDV. Our study highlights that SOM may misinterpret the physical mechanisms in the regions where ocean dynamics is important.

1
2
3
4
5
6
7
8
9
10
11
12
13
14
15
16
17
18
19
20

Deciphering the Role of Ocean Dynamics in Equatorial Pacific Decadal Variability

**Yu Zhang^{1,2}, Shi-Yun Yu^{1,3†}, Shang-Ping Xie⁴, Dillon J. Amaya^{5,6}, Qihua Peng⁷, Yu
Kosaka⁸, Xiaopei Lin^{1,2*}, Jun-Chao Yang^{1,2}, Sarah M. Larson⁹, Arthur J. Miller⁴, and Lei
Fan^{1,3}**

¹ Frontiers Science Center for Deep Ocean Multispheres and Earth System and Physical
Oceanography Laboratory, Ocean University of China, Qingdao, China

² Qingdao National Laboratory for Marine Science and Technology, Qingdao, China

³ College of Oceanic and Atmospheric Sciences, Ocean University of China, Qingdao, China

⁴ Scripps Institution of Oceanography, University of California San Diego, La Jolla, California

⁵ Cooperative Institute for Research in Environmental Sciences, University of Colorado Boulder,
Boulder, Colorado

⁶ Department of Atmospheric and Oceanic Sciences, University of Colorado Boulder, Boulder,
Colorado

⁷ State Key Laboratory of Tropical Oceanography, South China Sea Institute of Oceanology,
Chinese Academy of Sciences, Guangzhou, China

⁸ Research Center for Advanced Science and Technology, The University of Tokyo, Tokyo,
Japan

21 ⁹Department of Marine, Earth, and Atmospheric Sciences, North Carolina State University,
22 Raleigh, North Carolina

23

24 Corresponding author: Xiaopei Lin (linxiaop@ouc.edu.cn)

25 † The author contributed equally to this work.

26

27 **Key Points:**

- 28 • Thermodynamic-driven EPDV is primarily damped by equatorial Pacific mean
29 upwelling.
- 30 • The damped EPDV will be further amplified by anomalous ocean current.
- 31 • Slab ocean models may misinterpret the physical mechanisms in the regions where ocean
32 dynamics is important.

33 **Abstract**

34 Equatorial Pacific decadal variability (EPDV) modulates global climate. Although EPDV
35 is suggested to be generated by both air-sea thermodynamically coupled slab ocean models (SOM)
36 and fully coupled dynamic ocean models (DOM), the reason of EPDV simulated by the two
37 distinct hierarchies of models remains unclear. This ambiguity arises from a gap in the dynamical
38 framework between SOM and DOM. To fill the gap, we conducted a novel experiment (Clim- τ)
39 that retains only the effects of thermodynamic coupling and mean ocean current on EPDV (without
40 anomalous ocean current). We showed that in Clim- τ , thermodynamic-driven EPDV as in SOM
41 is largely damped by equatorial Pacific mean upwelling; whereas involving anomalous ocean
42 current as in DOM, the damped EPDV will be further amplified. Finally, we discussed the role of
43 ocean dynamics in the observed EPDV. Our study highlights that SOM may misinterpret the
44 physical mechanisms in the regions where ocean dynamics is important.

45

46 **Plain Language Summary**

47 The tropical Pacific impacts global climate. Decadal variability of tropical Pacific sea
48 surface temperatures (SST) in the equatorial belt features an El Niño/Southern Oscillation-like
49 SST pattern, which is termed equatorial Pacific decadal variability (EPDV) in this study. Previous
50 studies suggested that EPDV can be simulated by both simple air-sea thermodynamic coupled
51 models and more realistic fully coupled models; yet, the reason that it can be simulated by the two
52 different complexities of models remains unclear. To decipher this ambiguity, we conducted an
53 intermediate coupled model experiment, demonstrating that the above ambiguity is attributed to
54 the absence of the negative contribution from mean ocean current and positive contribution from

55 anomalous ocean current in the thermodynamic coupled models. We highlight that anomalous
56 ocean current could be the main driver for EPDV in the real world. Our study cautions that
57 thermodynamic coupled models may mislead the interpretation of real physical mechanism in the
58 regions where ocean dynamics is active.

59 **1 Introduction**

60 In the tropical Pacific, the El Niño-Southern Oscillation (ENSO) is the dominant mode of
61 ocean-atmosphere coupled variability on interannual timescales (Timmermann et al., 2018).
62 Additionally, the tropical Pacific also exhibits prominent ENSO-like variability on decadal
63 timescales, featuring meridionally broad sea surface temperature anomalies (SSTAs) in the
64 central-eastern Pacific (Chen & Wallace, 2015; Zhang et al., 1997). In this study, we focus on the
65 ENSO-like variability in 5°S-5°N equatorial Pacific, which is termed equatorial Pacific decadal
66 variability (EPDV). The EPDV has a profound impact on global climate. Specifically, the EPDV
67 modulates the rate of global mean surface temperature, resulting in the acceleration/slowdown of
68 the global warming rate (England et al., 2014; Kosaka & Xie, 2013, 2016; Yang et al., 2020).
69 Therefore, understanding the dynamical process of the EPDV is crucial for improving the
70 prediction of EPDV and the global climatic effects.

71 Unlike ENSO that originates from air-sea dynamic coupling (Timmermann et al., 2018),
72 the viewpoint supported by fully coupled dynamic ocean models (DOM), the EPDV can be
73 generated by both DOM (e.g., England et al., 2014; Li et al., 2016) and atmospheric models
74 coupled to motionless slab ocean models (SOM; Clement et al., 2011; Okumura, 2013; Zhang et
75 al., 2014) in which only air-sea thermodynamic coupling processes exist. The presence of EPDV
76 in SOM has been shown to originate in the southeast Pacific (Okumura, 2013; Zhang et al., 2014),
77 the SSTAs therein propagating onto the equator via the wind-evaporation-SST (WES) feedback
78 (Xie & Philander, 1994).

79 The EPDV simulated in both DOM and SOM motivates us to address the questions: why
80 can it be generated by the two distinct hierarchies of modeling experiments? Does ocean dynamics

81 play a role in EPDV? If does, then what role does ocean dynamics play? These questions, however,
82 are hardly answered, perhaps arising from a gap in the dynamical framework between SOM and
83 DOM (Larson et al., 2018a). Specifically, compared to SOM, DOM includes effects of both mean
84 and anomalous ocean current on SSTAs. Removing either effect would thus fill the dynamical gap
85 between SOM and DOM, benefiting to answer the above questions.

86 To fill the dynamical gap, we conducted a novel air-sea partial coupling experiment, named
87 Clim- τ , in which climatological wind stresses are prescribed over the tropical Pacific. As a result,
88 the experiment suppresses anomalous ocean current driven by the anomalous wind stress, but
89 retains the effect of mean ocean current as well as air-sea thermodynamic coupling processes on
90 EPDV. Consequently, by comparing SOM to Clim- τ , we explored the role of mean ocean current
91 in EPDV; by comparing Clim- τ to DOM, we investigated the role of anomalous ocean current in
92 EPDV. Our results showed that 1) in SOM, thermodynamic coupling processes without ocean
93 current indeed leads to EPDV; 2) in Clim- τ , equatorial Pacific mean upwelling damps the
94 thermodynamic-driven EPDV; 3) in DOM, anomalous ocean current amplifies or even overcomes
95 the upwelling-damped EPDV. Our study demonstrates that although both SOM and DOM simulate
96 similar EPDV pattern to observations, SOM may misinterpret the physical mechanism in the
97 equatorial Pacific where ocean dynamics is important.

98

99 **2 Data**

100 **2.1 A Hierarchy of Coupled Model Experiments**

101 We investigated the roles of mean and anomalous ocean current in EPDV via a step-by-
102 step comparison among SOM, Clim- τ , and DOM. All the model experiments were based on the

103 Geophysical Fluid Dynamic Laboratory coupled model version 2.1 (CM2.1; Delworth et al., 2006).
104 The models consist of the atmospheric model version 2.1 (AM2.1) with horizontal resolution of
105 2.5° longitude \times 2° latitude, and the Modular Ocean Model version 4.1 with horizontal resolution
106 of 1° longitude \times 1° latitude poleward of 30° . The latitudinal resolution equatorward of 30° in the
107 ocean model gets gradually finer to $1/3^\circ$ at the equator.

108 For the SOM, we used a motionless, constant-depth slab ocean coupled with AM2.1, which
109 isolates to only retain thermodynamic coupling processes without ocean dynamics. The length of
110 the SOM experiment was 100 years; mixed layer depth was fixed at 50 m globally.

111 For the Clim- τ , we prescribed wind stresses over the tropical Pacific with daily
112 climatological values obtained from a 1000-year DOM (described below). The prescribed region
113 is 15°S - 15°N with 10° buffer zone north and south where the simulated and prescribed wind
114 stresses are blended, with the weight linearly tapering off (see Figure 1 of Zhang et al., 2021). In
115 order to suppress tiny day-to-day fluctuations that remain in the 1000-year climatology, the
116 prescribed wind stress had been weakly smoothed temporally by removing the annual harmonics
117 higher than 18 (corresponding to a frequency of about 20 days). This Clim- τ experiment is the
118 same as mechanically decoupling the DOM (Larson & Kirtman, 2015; Larson et al., 2018a, 2018b),
119 except that only the tropical Pacific is mechanically decoupled. Outside the tropical Pacific, the
120 ocean and atmosphere are fully coupled and free to evolve. The Clim- τ experiment was integrated
121 for 310 years, and only the last 300 years were analyzed. This experiment was recently used to
122 investigate the Pacific Meridional Modes (Amaya, 2019; Amaya et al., 2019; Chiang & Vimont,
123 2004) without equatorial Pacific influence by Zhang et al. (2021). They discussed the damped
124 equatorial Pacific variability in the Clim- τ was attributed to the mean equatorial upwelling driven

125 by the mean trade winds. In this study, we will explicitly show how the mean equatorial Pacific
126 upwelling plays a key role in damping EPDV.

127 Finally, we integrated a 1000-year DOM, which includes both buoyancy (thermodynamic
128 and freshwater flux) and dynamic coupling globally. For the dynamic coupling, DOM contains the
129 effects of both mean and anomalous wind-driven ocean current and their impact on SSTAs. It also
130 contains other ocean processes, such as mixing, diffusion, and entrainment.

131 **2.2 Observational Data**

132 We also used observational data to explore the role of ocean dynamics in EPDV. We used
133 monthly SST datasets from the Hadley Centre Global Sea Ice and Sea Surface Temperature version
134 1.1 (HadISSTv1.1; Rayner et al., 2003) and the NOAA Extended Reconstructed SST version 5
135 (ERSSTv5; Huang et al., 2017). The horizontal resolution of the HadISSTv1.1 is $1^\circ \times 1^\circ$ and of
136 the ERSSTv5 is $2^\circ \times 2^\circ$. We also used monthly surface heat flux variables (including shortwave,
137 longwave, sensible, and latent heat fluxes) of atmospheric reanalysis dataset from the NOAA-
138 CIRES-DOE Twentieth Century Reanalysis version 3 (20CRv3; Slivinski et al., 2019) with $1^\circ \times$
139 1° horizontal resolution. All the above data are from 1900 to 2015. Monthly anomaly data are
140 obtained by removing 1900-2015 monthly climatology and linear trend.

141

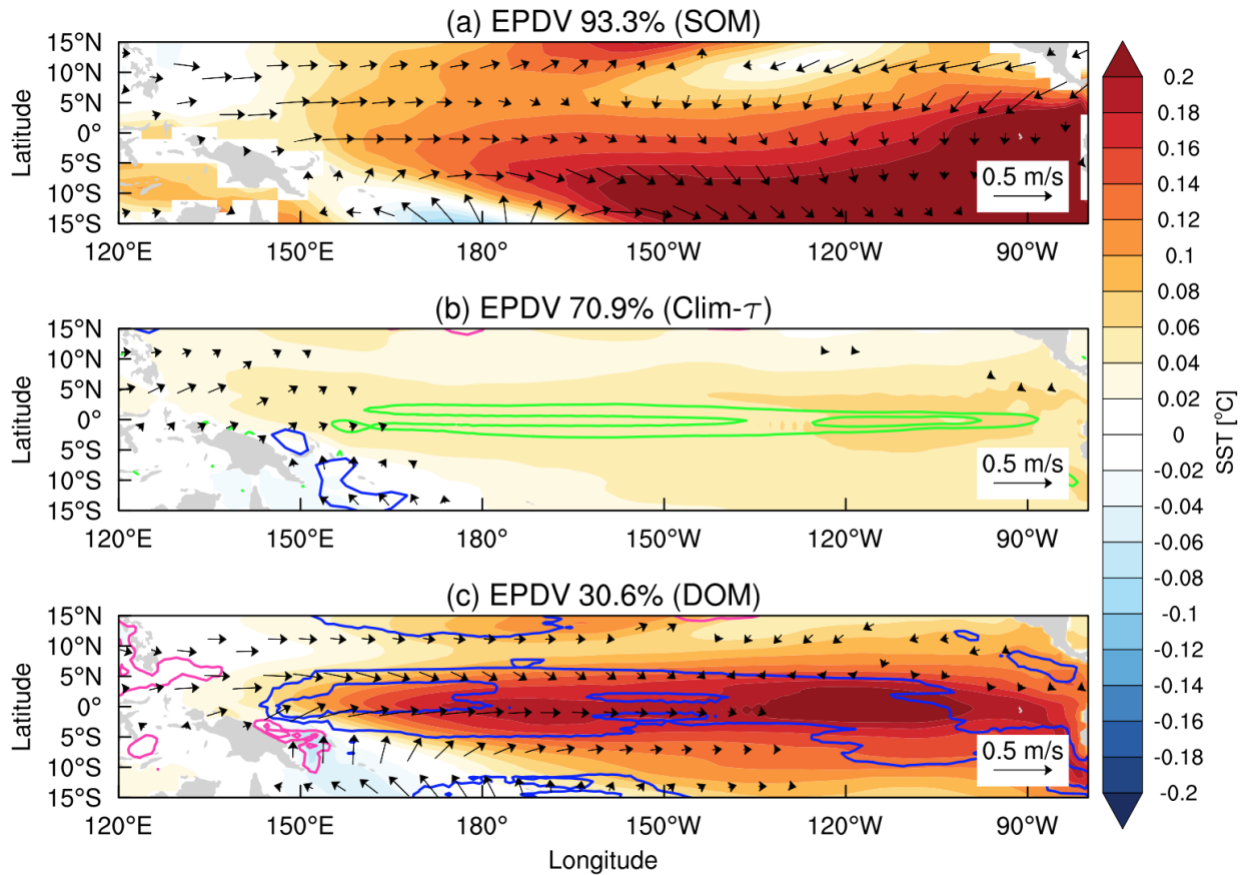
142 **3 Results**

143 **3.1 EPDV in a Hierarchy of Coupled Model Simulations**

144 We explore the roles of mean and anomalous ocean current in EPDV via a step-by-step
145 comparison among the SOM, Clim- τ , and DOM. The EPDV is defined as the first empirical
146 orthogonal function mode (EOF1) of 20-year low-pass filtered annual-mean SSTAs in 5°S - 5°N

147 equatorial Pacific, except for the DOM in which the EPDV emerges as the second EOF mode
 148 (EOF1 exhibits a zonal dipole pattern, related to ENSO amplitude decadal modulation; Ogata et
 149 al., 2013; Rodgers et al., 2004; Yeh & Kirtman, 2004; Fig. S1). The applied 20-year low-pass filter
 150 was to largely remove interannual ENSO variability. Patterns in Figure 1 display the regression
 151 maps of SST, surface wind, and surface net heat flux anomalies against the corresponding
 152 normalized principal component (PC) of EPDV in each experiment.

153



154

155 **Figure 1. EPDV patterns in the three experiments.** Regression maps of SST (shading; °C),
 156 surface wind (vectors; m s⁻¹), and surface net heat flux anomalies (contour interval: 1 W m⁻²; purple
 157 is positive and blue is negative; downward positive) against the normalized PC time series of

158 EPDV. (a) SOM, (b) Clim- τ (mean upwelling velocity is green contour), and (c) DOM. The
159 explained variance of EPDV for each experiment is labeled in the title.

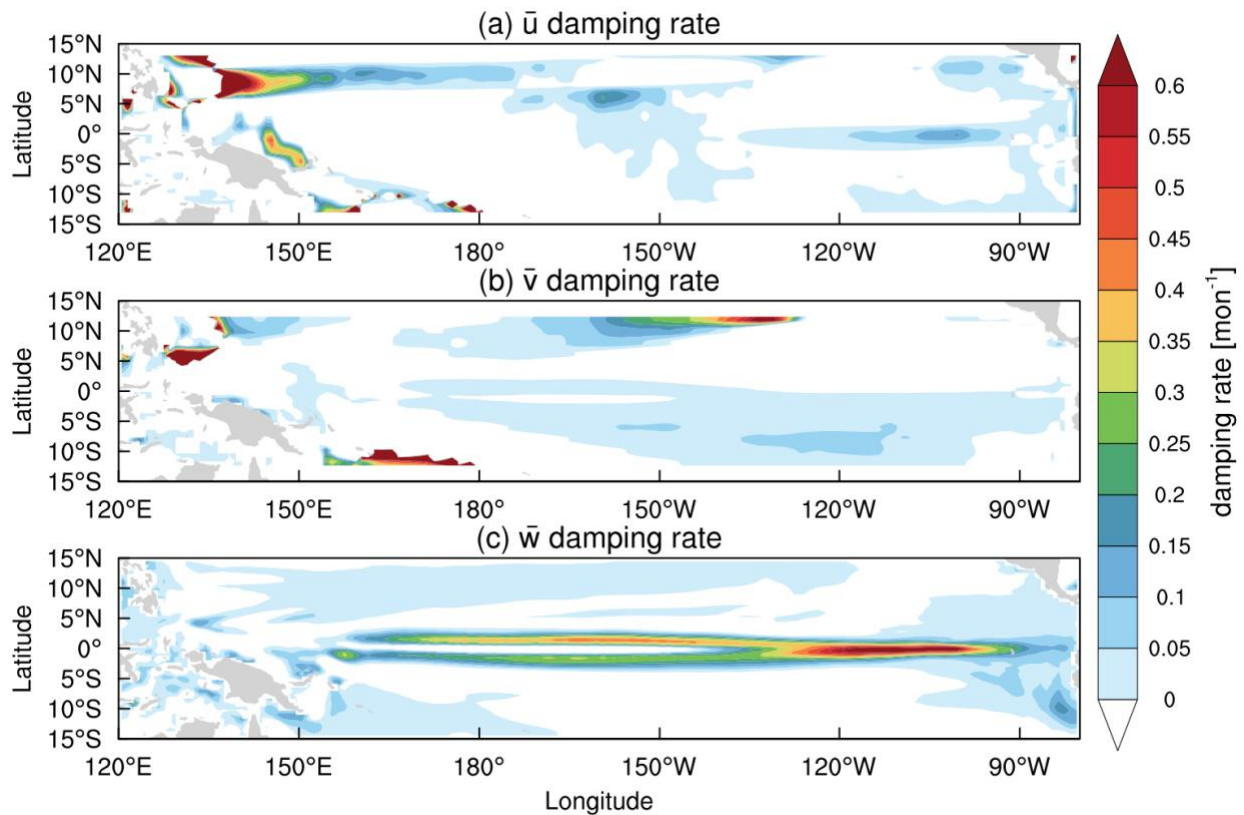
160

161 The results show that in the SOM (Fig. 1a), EPDV exhibits strong SSTAs in the southeast
162 Pacific and moderate SSTAs in the northeast Pacific. This equatorial asymmetry in the SSTAs
163 mainly results from the distinct intensify of the WES feedbacks in the two hemispheres (Fig. S2).
164 The SSTAs strongly correlate with surface wind anomalies, which are characterized by westerly
165 anomalies over the central Pacific and cross-equatorial northerly anomalies flowing towards the
166 southeast Pacific. The EPDV in the SOM resembles that simulated in other SOMs (Okumura,
167 2013; Zhang et al., 2014). Previous studies pointed out that EPDV in SOMs originates from the
168 southeast Pacific SSTAs that propagate onto the equator primarily through the WES feedback
169 (Zhang et al., 2014). Note that on decadal timescales, changes in the upper ocean temperature are
170 in a quasi-equilibrium (i.e., all the processes that force SSTAs are balanced with all the damping
171 processes). As a result, net surface heat flux anomaly associated with the EPDV in the SOM is
172 rather weak (no contours in Fig. 1a) because it is the only driver for SSTAs.

173 Surprisingly, in the Clim- τ (Fig. 1b), EPDV-related SSTAs are markedly damped. Due to
174 the same thermodynamic coupling processes as in the SOM, this damping is only attributed to the
175 effect of mean ocean current. To further investigate which dimension of mean ocean current
176 dominantly damps EPDV, we estimate the damping rate of each dimension of mean ocean current
177 acting on the EPDV-associated SSTAs. The damping rate is computed by the EPDV-associated
178 SSTAs (pattern of Fig. 1a) gradient advected by annual-mean ocean current (obtained from the
179 Clim- τ) divided by the EPDV-associated SSTAs. The result shows that anomalous ocean
180 advections by all three-dimensional mean ocean currents damp the EPDV-related SSTAs off the

181 equatorial Pacific (Fig. 2). The SSTAs on the equatorial Pacific (i.e., the EPDV), in contrast, are
 182 predominantly damped by the climatological upwelling (Fig. 2c). The estimated damping rate of
 183 the mean upwelling on the equator is about $0.2\text{-}0.6\text{ mon}^{-1}$, indicating its critical role in damping
 184 the EPDV.

185



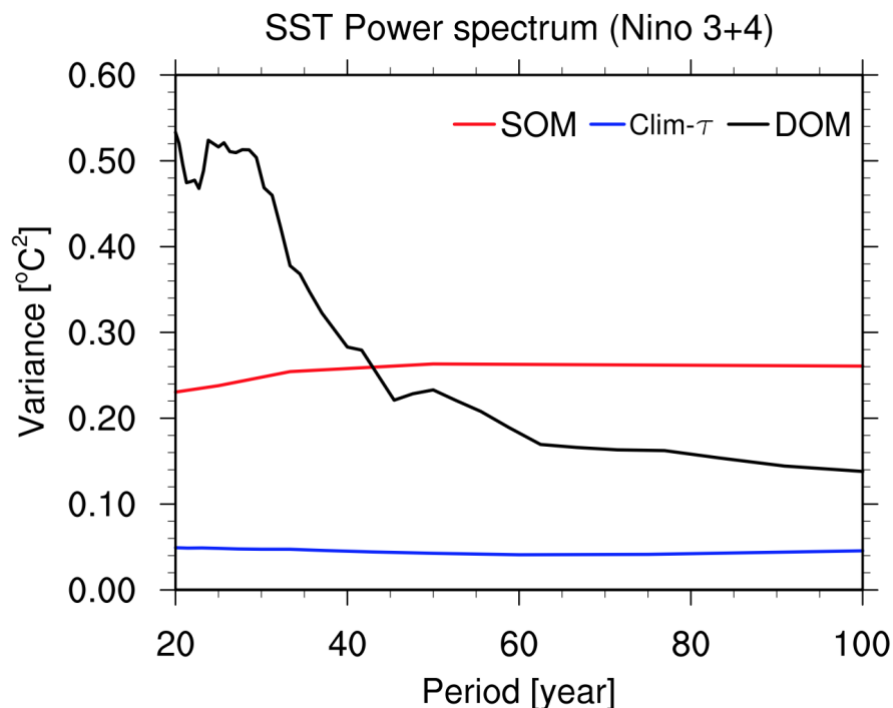
186

187 **Figure 2. Estimated EPDV damping rate in the Clim- τ .** (a)-(c) Patterns of the estimated
 188 damping rate (see the method in text; unit: mon^{-1}) by annual-mean climatological zonal,
 189 meridional, and 50-m vertical current, respectively. All the climatological currents are from the
 190 Clim- τ experiment. Negative values (representing forcing rate) are set to white colors.

191

192 This dominant damping effect by equatorial Pacific mean upwelling, in fact, acts not only
 193 on decadal but also on inter-decadal to multi-decadal timescales. To illustrate this point, we
 194 perform power spectrum analysis of annual-mean SSTAs averaged over the Niño-3 plus Niño-4
 195 regions (160°E-90°W, 5°S-5°N) in each experiment. SSTAs averaged over this region will largely
 196 remove the signal of zonal dipole mode in the DOM and represent EPDV in all experiments (Fig.
 197 S3). The result shows that in the SOM, EPDV variance gradually increases longer than 20-year
 198 period and then stabilizes at 0.26 °C² after 40-year period (red line in Fig. 3). This relatively
 199 stabilized EPDV variance longer than decadal timescales reflects a reddened spectrum generated
 200 by integrating atmospheric white noise forcing (Clement et al., 2011; Frankignoul & Hasselmann,
 201 1977; Okumura, 2013). EPDV variance in the Clim- τ , in contrast, decreases by ~80% compared
 202 to that in the SOM (blue line in Fig. 3), indicating the prominent role of mean upwelling in damping
 203 equatorial Pacific SSTAs on decadal to multi-decadal timescales.

204



205

206 **Figure 3. Power spectra of EPDV in the three experiments.** The power spectra (unit: $^{\circ}\text{C}^2$) are
207 performed based on the annual-mean SSTAs averaged over Niño-3 plus Niño-4 regions in each
208 experiment. Spectra with periods no less than 20 years are shown. Red: SOM; blue: Clim- τ ; black:
209 DOM.

210

211 Compared to the EPDV in the Clim- τ , EPDV is intensified in the DOM (Fig. 1c),
212 suggesting that anomalous ocean current plays a role in amplifying the EPDV. The strength of the
213 amplification, however, is distinct on different timescales (black line in Fig. 3). Specifically, the
214 amplification is strong on inter-decadal (20~40 years) timescales, leading to the EPDV variance
215 in the DOM larger than that in the SOM. In contrast, the strength of the amplification becomes
216 gradually weak on multi-decadal (>40 years) timescales, resulting in the EPDV variance in the
217 DOM smaller than that in the SOM. This timescale-dependent amplification strength seems to be
218 in line with the theoretical study by Clarke (2010), which pointed out that longer timescales, weaker
219 interactive ocean dynamics in the eastern equatorial Pacific (i.e., weaker amplification strength).

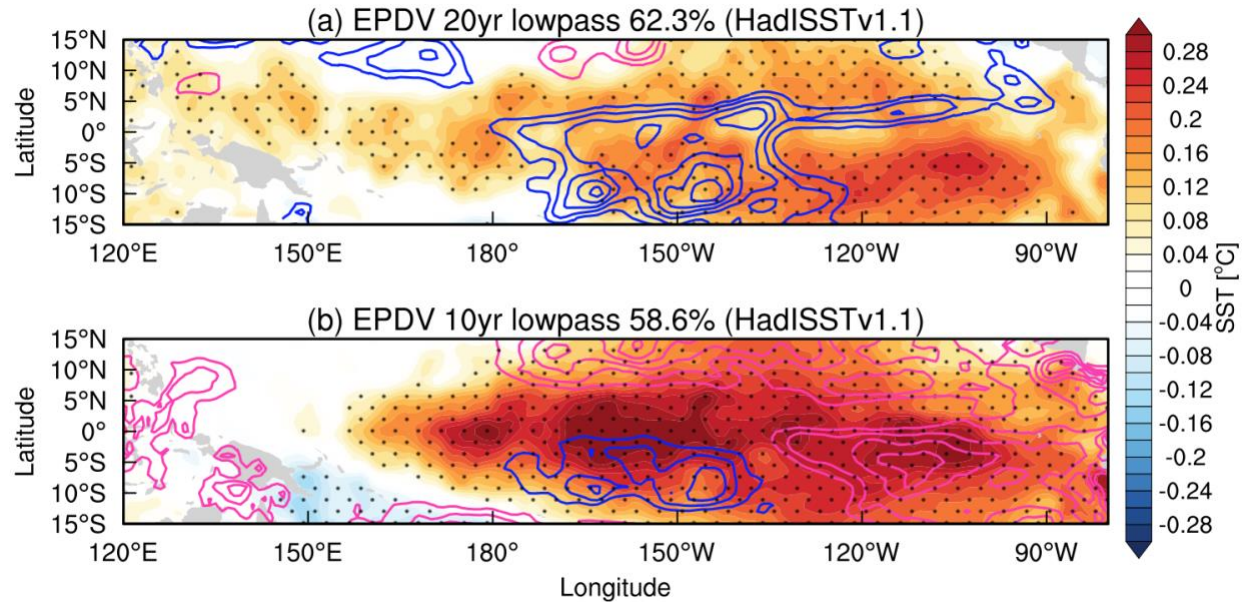
220 Further, EPDV in the DOM is damped by net surface heat flux (blue contours in Fig. 1c).
221 Together with the dynamical damping by the equatorial Pacific mean upwelling revealed from the
222 Clim- τ , EPDV is driven by the effect of anomalous ocean current, rather than air-sea
223 thermodynamic coupling as seen in the SOM.

224 **3.2 EPDV in observations**

225 Here we discuss the roles of mean and anomalous ocean current in the observed EPDV.
226 The mean ocean current is supposed to play a damping role, primarily by equatorial Pacific mean
227 upwelling, the result inferred from the Clim- τ . The anomalous ocean current, in contrast, plays a

228 forcing role in most of the equatorial Pacific regions, the result inferred from the negative net
229 surface heat flux anomalies between 180° and 100°W (Fig. 4a). As a caveat, this result may be
230 insignificant as the EPDV obtained from the EOF1 of 20-year low-pass filtered annual-mean
231 SSTAs in the equatorial Pacific does not exceed the 95% confidence level due to the limited
232 degrees of freedom in observations. Thus, alternatively, we extract “EPDV” by performing EOF
233 analysis with 10-year low-pass filtered annual-mean SSTAs. The resulting “EPDV” is significant
234 at the 95% confidence level, with weak negative net surface heat flux anomalies in the central
235 equatorial Pacific (180°-135°W) and strong positive net surface heat flux anomalies in the eastern
236 equatorial Pacific (east of 135°W) (Fig. 4b). The weak negative net surface heat flux anomalies in
237 the central equatorial Pacific implies that anomalous ocean current plays a forcing role, offsetting
238 the damping effects of the weak net heat flux and mean upwelling. The strong positive net surface
239 heat flux anomalies in the eastern equatorial Pacific may largely counteract the strong damping
240 effect by mean upwelling, resulting in a weak role of anomalous ocean current played therein. The
241 above analyses are also seen if based on ERSSTv5 dataset (Fig. S4). To the extent of the role of
242 anomalous ocean current in the observed EPDV needs to be quantified in future studies.

243



244

245 **Figure 4. EPDV patterns in observations.** The observed EPDV patterns shown are based on the
 246 HadISSTv1.1. (a) As in Fig. 1, (b) EPDV is denoted as EOF1 of 10-year low-pass filtered annual-
 247 mean SSTAs in the equatorial Pacific. Stippling in (a) and (b) denote the regressed SSTAs (shading)
 248 significant at the 95% confidence level. The regressed net surface heat flux anomalies (contours)
 249 only significant at the 95% confidence level are shown. Both significance tests are based on the
 250 two-tailed F test.

251

252 4 Summary and Discussion

253 To fill the gap between the air-sea thermodynamic coupled SOM and fully coupled DOM,
 254 we conducted a partial coupling experiment—Clim- τ —which retains the effects of air-sea
 255 thermodynamic coupling and mean ocean current driven by mean wind stress on SSTAs. With a
 256 step-by-step comparison among the SOM, Clim- τ , and DOM based on the CM2.1, we have
 257 investigated the roles of mean and anomalous ocean current in EPDV. We showed that mean ocean

258 current, primarily the equatorial Pacific mean upwelling, plays a key role in damping EPDV.
259 Anomalous ocean current in turn, amplifies the damped EPDV and even overwhelms the damping
260 effect by mean ocean current, leading to a role in forcing EPDV. Finally, we discussed the role of
261 ocean current in the observed EPDV.

262 Our study demonstrates that SOMs may misinterpret the physical mechanism in the regions
263 where mean upwelling is prominent. Apart from the mean upwelling regions, climate phenomena
264 in others regions with strong ocean dynamics were also simulated by SOMs. For example, in the
265 North Atlantic, the Atlantic Multi-decadal Variability (AMV; Sutton et al., 2018; Zhang et al.,
266 2019), which was thought to be strongly related to the Atlantic Meridional Overturning Circulation
267 (Buckley & Marshall, 2016; Kuhlbrodt et al., 2007), was recently challenged by SOM simulations
268 (Clement et al., 2015). Despite the similarity of the AMV patterns between SOM and DOM on the
269 ocean surface, other AMV-related patterns in the subsurface, such as the temperature anomaly
270 structure, are distinct (Zhang et al., 2019). The examples of the AMV and our EPDV studies
271 caution against the overuse of SOMs in revealing the physical mechanisms of climate phenomena
272 in the regions where ocean dynamics is active.

273 **Acknowledgments**

274 The HadISSTv1.1 data is available at
275 <https://www.metoffice.gov.uk/hadobs/hadisst/data/download.html>. The ERSSTv5 data is
276 available at <https://psl.noaa.gov/data/gridded/data.noaa.ersst.v5.html>. The 20CRv3 data is
277 available at https://psl.noaa.gov/data/gridded/data.20thC_ReanV3.html#detail. The SOM data is
278 available at [https://nomads.gfdl.noaa.gov/dods-data/gfdl_sm2_1/MLM2.1U_Control-](https://nomads.gfdl.noaa.gov/dods-data/gfdl_sm2_1/MLM2.1U_Control-1990_D1/pp/atmos/ts/monthly/)
279 [1990_D1/pp/atmos/ts/monthly/](https://nomads.gfdl.noaa.gov/dods-data/gfdl_sm2_1/MLM2.1U_Control-1990_D1/pp/atmos/ts/monthly/); the Clim- τ data is available at
280 <https://data.mendeley.com/datasets/ctn5k77ttr/draft?a=c9db68b4-d4af-48a4-b14d-709edc7fa1b7>;
281 the DOM data is available at [https://data.mendeley.com/datasets/mrg8g4w9zk/draft?a=4d2e535f-](https://data.mendeley.com/datasets/mrg8g4w9zk/draft?a=4d2e535f-7dc6-4f10-b2ad-c1bf565637ce)
282 [7dc6-4f10-b2ad-c1bf565637ce](https://data.mendeley.com/datasets/mrg8g4w9zk/draft?a=4d2e535f-7dc6-4f10-b2ad-c1bf565637ce). Y.Z. and X.L. were supported by the National Natural Science
283 Foundation of China (92058203 and 41925025). D.J.A. was funded under a CIRES Postdoctoral
284 Fellowship at CU Boulder. Q.P. was supported by the National Natural Science Foundation of
285 China (42005035) and the Independent Research Project Program of State Key Laboratory of
286 Tropical Oceanography (LTOZZ2102). Y.K. was supported by the Japan Society for the
287 Promotion of Science (JP18H01278, JP18H01291 and JP19H05703), the Japanese Ministry of
288 Education, Culture, Sports, Science and Technology (JPMXD0717935457 and
289 JPMXD1420318865), and the Environmental Restoration and Conservation Agency of Japan
290 (JPMEERF20192004). J.-C.Y. was supported by the project funded by China Postdoctoral
291 Science Foundation (2020M672138) and the Fundamental Research Funds for the Central
292 Universities (202013029). S.M.L. was supported by the National Science Foundation (AGS-
293 1951713). A.J.M. was supported by the National Science Foundation (OCE2022868 and CCE-
294 LTER OCE1637632) and NOAA (MAPP NA17OAR4310106). L.F. was supported by the
295 Natural Science Foundation of China (41975089).

296 **References**

- 297 Amaya, D. J. (2019). The Pacific Meridional Mode and ENSO: A review. *Current Climate*
298 *Change Reports*, 5, 296–307. <https://doi.org/10.1007/s40641-019-00142-x>
- 299 Amaya, D. J., Kosaka, Y., Zhou, W., Zhang, Y., Xie, S.-P. & Miller, A. J. (2019). The North
300 Pacific pacemaker effect on historical ENSO and its mechanisms. *Journal of Climate*, 32,
301 7643–7661. <https://doi.org/10.1175/JCLI-D-19-0040.1>
- 302 Buckley, M. W., & Marshall, J. (2016). Observations, inferences, and mechanisms of the
303 Atlantic Meridional Overturning Circulation: A review. *Reviews of Geophysics*, 54, 5–63.
304 <https://doi.org/10.1002/2015RG000493>
- 305 Chen, X., & Wallace, J. M. (2015). ENSO-like variability: 1900–2013. *Journal of Climate*, 28,
306 9623–9641. <https://doi.org/10.1175/JCLI-D-15-0322.1>
- 307 Chiang, J., & Vimont, D. J. (2004). Analogous Pacific and Atlantic meridional modes of tropical
308 atmosphere–ocean variability. *Journal of Climate*, 17, 4143–4158.
309 <https://doi.org/10.1175/JCLI4953.1>
- 310 Clarke, A. J. (2010). Analytical Theory for the Quasi-Steady and Low-Frequency Equatorial
311 Ocean Response to Wind Forcing: The “Tilt” and “Warm Water Volume” Modes.
312 *Journal of Physical Oceanography*, 40, 121-137. <https://doi.org/10.1175/2009JPO4263.1>
- 313 Clement, A., Bellomo, K., Murphy, L. N., Cane, M. A., Mauritsen, T., Rädcl, G., & Stevens, B.
314 (2015). The Atlantic Multidecadal Oscillation without a role for ocean circulation.
315 *Science*, 350(6258), 320–324. <https://doi.org/10.1126/science.aab3980>

- 316 Clement, A., Di Nezio, P., & Deser, C. (2011). Rethinking the ocean's role in the Southern
317 Oscillation. *Journal of Climate*, 24, 4056–4072. <https://doi.org/10.1175/2011JCLI3973.1>
- 318 Delworth, T. L., Broccoli, A. J., Rosati, A., Stouffer, R. J., Balaji, V., Beesley, J. A., et al.
319 (2006). GFDL's CM2 global coupled climate models. Part I: Formulation and simulation
320 characteristics. *Journal of Climate*, 13, 643–674. <https://doi.org/10.1175/JCLI3629.1>
- 321 England, M. H., McGregor, S., Spence, P., Meehl, G. A., Timmermann, A., Cai, W., et al.
322 (2014). Recent intensification of wind-driven circulation in the Pacific and the ongoing
323 warming slowdown. *Nature Climate Change*, 4, 222–227 (2014).
324 <https://doi.org/10.1038/nclimate2106>
- 325 Frankignoul, C., & Hasselmann, K. (1977). Stochastic climate models. Part II: Application to
326 sea-surface temperature anomalies and thermocline variability. *Tellus*, 29A, 289–305,
327 <https://doi.org/10.1111/j.2153-3490.1977.tb00740.x>.
- 328 Huang, B., Thorne, P. W., Banzon, V. F., Boyer, T., Chepurin, G., Lawrimore, J. H., et al.
329 (2017). Extended reconstructed sea surface temperature, version 5 (ERSSTv5): upgrades,
330 validations, and intercomparisons. *Journal of Climate*, 30(20), 8179-8205.
331 <https://doi.org/10.1175/JCLI-D-16-0836.1>
- 332 Kosaka, Y., & Xie, S.-P. (2013). Recent global-warming hiatus tied to equatorial Pacific surface
333 cooling. *Nature*, 501, 403–407. <https://doi.org/10.1038/nature12534>
- 334 Kosaka, Y., & Xie, S.-P. (2016). The tropical Pacific as a key pacemaker of the variable rates of
335 global warming. *Nature Geoscience*, 9, 669–673. <https://doi.org/10.1038/ngeo2770>
- 336

- 337 Kuhlbrodt, T., Griesel, A., Montoya, M., Levermann, A., Hofmann, M., & Rahmstorf, S. (2007).
338 On the driving processes of the Atlantic meridional overturning circulation. *Reviews of*
339 *Geophysics*, 45, RG2001. <https://doi.org/10.1029/2004RG000166>
- 340 Larson, S. M., & Kirtman, B. P. (2015). Revisiting ENSO coupled instability theory and SST
341 error growth in a fully coupled model. *Journal of Climate*, 28, 4724–4742.
342 <https://doi.org/10.1175/JCLI-D-14-00731.1>
- 343 Larson, S. M., Vimont, D. J., Clement, A., & Kirtman, B. P. (2018a). How momentum coupling
344 affects SST variance and large-scale Pacific climate variability in CESM. *Journal of*
345 *Climate*, 31, 2927-2944. <https://doi.org/10.1175/JCLI-D-17-0645.1>
- 346 Larson, S. M., Pegion, K. V., & Kirtman, B. P. (2018b). The South Pacific meridional mode as a
347 thermally driven source of ENSO amplitude modulation and uncertainty. *Journal of*
348 *Climate*, 31, 5127-5145. <https://doi.org/10.1175/JCLI-D-17-0722.1>
- 349 Li, X., Xie, S.-P., Gille, S. T., & Yoo, C. (2016). Atlantic-induced pan-tropical climate change
350 over the past three decades. *Nature Climate Change*, 6, 275–279.
351 <https://doi.org/10.1038/nclimate2840>
- 352 Ogata, T., Xie, S.-P., Wittenberg, A., & Sun, D. Z. (2013). Interdecadal amplitude modulation of
353 El Niño–Southern Oscillation and its impact on tropical Pacific decadal variability.
354 *Journal of Climate*, 26, 7280-7297. <https://doi.org/10.1175/JCLI-D-12-00415.1>
- 355 Okumura, Y. M. (2013). Origins of tropical Pacific decadal variability: Role of stochastic
356 atmospheric forcing from the South Pacific. *Journal of Climate*, 26, 9791–9796.
357 <https://doi.org/10.1175/JCLI-D-13-00448.1>

- 358 Rayner, N. A., Parker, D. E., Horton, E. B., Folland, C. K., Alexander, L. V., Rowell, D. P.,
359 Kent, E. C. & Kaplan, A. (2003). Global analyses of sea surface temperature, sea ice, and
360 night marine air temperature since the late nineteenth century. *Journal of Geophysical*
361 *Research: Atmospheres*, 108, 4407. <https://doi.org/10.1029/2002JD002670>
- 362 Rodgers, K. B., Friederichs, P., & Latif, M. (2004). Tropical Pacific decadal variability and its
363 relation to decadal modulations of ENSO. *Journal of Climate*, 17, 3761-3774.
364 [https://doi.org/10.1175/1520-0442\(2004\)017<3761:TPDVAI>2.0.CO;2](https://doi.org/10.1175/1520-0442(2004)017<3761:TPDVAI>2.0.CO;2)
- 365 Slivinski, L. C., Compo, G. P., Whitaker, J. S., Sardeshmukh, P. D., Giese, B. S., McColl, C., et
366 al. (2019). Towards a more reliable historical reanalysis: Improvements for version 3 of
367 the Twentieth Century Reanalysis system. *Quarterly Journal of the Royal Meteorological*
368 *Society*, 145(724), 2876-2908. <https://doi.org/10.1002/qj.3598>
- 369 Sutton, R. T., McCarthy, G. D., Robson, J., Sinha, B., Archibald, A. T., & Gray, L. J. (2018).
370 Atlantic multidecadal variability and the UK ACSIS program. *Bulletin of the American*
371 *Meteorological Society*, 99(2), 415–425. <https://doi.org/10.1175/BAMS-D-16-0266.1>
- 372 Timmermann, A., An, S.-I., Kug, J.-S., Jin, F.-F., Cai, W., Capotondi, A., et al. (2018). El Niño–
373 Southern Oscillation complexity. *Nature*, 559, 535–545. [https://doi.org/10.1038/s41586-](https://doi.org/10.1038/s41586-018-0252-6)
374 [018-0252-6](https://doi.org/10.1038/s41586-018-0252-6)
- 375 Xie, S.-P., & Philander, S. G. H. (1994). A coupled ocean-atmosphere model of relevance to the
376 ITCZ in the eastern Pacific. *Tellus*, 46A, 340–350.
377 <https://doi.org/10.3402/tellusa.v46i4.15484>

- 378 Yang, J.-C., Lin, X., Xie, S.-P., Zhang, Y., Kosaka, Y., & Li, Z. (2020). Synchronized tropical
379 Pacific and extratropical variability during the past three decades. *Nature Climate*
380 *Change*, *10*(5), 422-427. <https://doi.org/10.1038/s41558-020-0753-9>
- 381 Yeh, S.-W., & Kirtman, B. P. (2004). Tropical Pacific decadal variability and ENSO amplitude
382 modulation in a CGCM. *Journal of Geophysical Research*, *109*, C11.
383 <https://doi.org/10.1029/2004JC002442>
- 384 Zhang, H., Clement, A., & Di Nezio, P. (2014). The South Pacific meridional mode: A
385 mechanism for ENSO-like variability. *Journal of Climate*, *27*, 769-783.
386 <https://doi.org/10.1175/JCLI-D-13-00082.1>
- 387 Zhang, R., Sutton, R., Danabasoglu, G., Kwon, Y.-O., Marsh, R., Yeager, S. G., et al. (2019). A
388 review of the role of the Atlantic meridional overturning circulation in Atlantic
389 multidecadal variability and associated climate impacts. *Reviews of Geophysics*, *57*(2),
390 316-375. <https://doi.org/10.1029/2019RG000644>
- 391 Zhang, Y., Wallace, J. M., & Battisti, D. S. (1997). ENSO-like interdecadal variability: 1900–93.
392 *Journal of Climate*, *10*, 1004–1020. [https://doi.org/10.1175/1520-](https://doi.org/10.1175/1520-0442(1997)010<1004:ELIV>2.0.CO;2)
393 [0442\(1997\)010<1004:ELIV>2.0.CO;2](https://doi.org/10.1175/1520-0442(1997)010<1004:ELIV>2.0.CO;2)
- 394 Zhang, Y., Yu, S., Amaya, D. J., Kosaka, Y., Larson, S. M., Wang, X., et al. (2021). Pacific
395 Meridional Modes without equatorial Pacific influence. *Journal of Climate*, *34*, 5285–
396 5301. <https://doi.org/10.1175/JCLI-D-20-0573.1>

Deciphering the Role of Ocean Dynamics in Equatorial Pacific Decadal Variability

Yu Zhang^{1,2}, Shi-Yun Yu^{1,3†}, Shang-Ping Xie⁴, Dillon J. Amaya^{5,6}, Qihua Peng⁷, Yu Kosaka⁸, Xiaopei Lin^{1,2*}, Jun-Chao Yang^{1,2}, Sarah M. Larson⁹, Arthur J. Miller⁴, and Lei Fan^{1,3}

¹ Frontiers Science Center for Deep Ocean Multispheres and Earth System and Physical Oceanography Laboratory, Ocean University of China, Qingdao, China

² Qingdao National Laboratory for Marine Science and Technology, Qingdao, China

³ College of Oceanic and Atmospheric Sciences, Ocean University of China, Qingdao, China

⁴ Scripps Institution of Oceanography, University of California San Diego, La Jolla, California

⁵ Cooperative Institute for Research in Environmental Sciences, University of Colorado Boulder, Boulder, Colorado

⁶ Department of Atmospheric and Oceanic Sciences, University of Colorado Boulder, Boulder, Colorado

⁷ State Key Laboratory of Tropical Oceanography, South China Sea Institute of Oceanology, Chinese Academy of Sciences, Guangzhou, China

⁸ Research Center for Advanced Science and Technology, The University of Tokyo, Tokyo, Japan

⁹ Department of Marine, Earth, and Atmospheric Sciences, North Carolina State University, Raleigh, North Carolina

Contents of this file

Figures S1 to S4

Additional Supporting Information (Files uploaded separately)

None

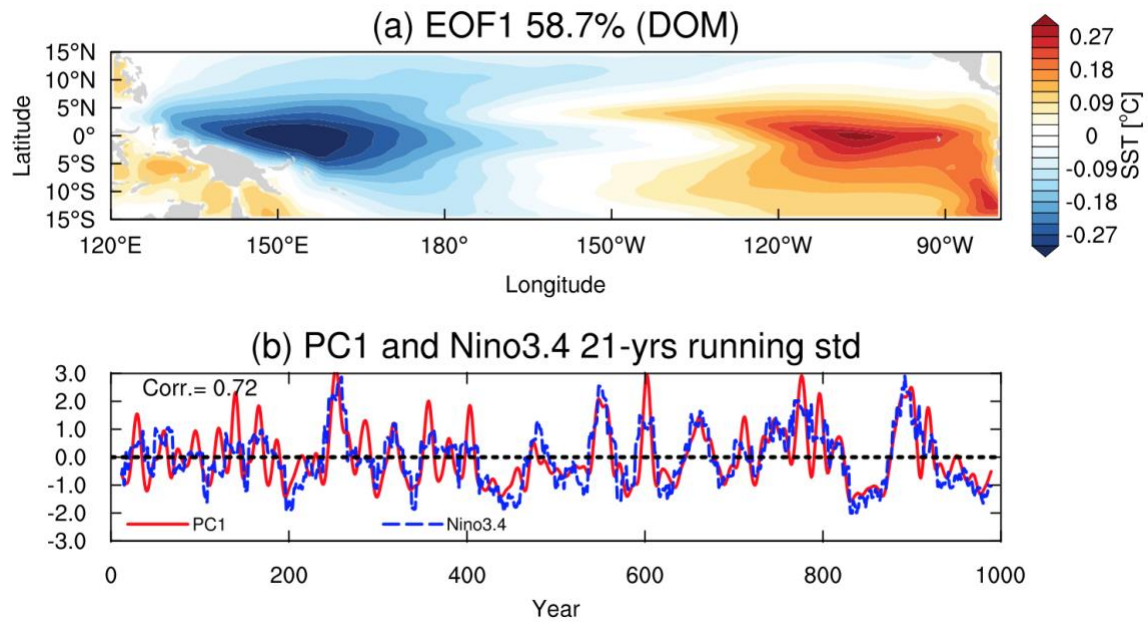


Figure S1. Zonal dipole mode in the DOM. (a) EOF1 of 20-year low-pass filtered annual-mean SSTAs in the equatorial Pacific. (b) The corresponding normalized PC (solid red line) with normalized 21-year running standard deviation of November-January SSTAs averaged over the Niño-3.4 region (170°W-120°W, 5°S-5°N) (dashed blue line). The correlation coefficient between the two time series is labeled in the panel.

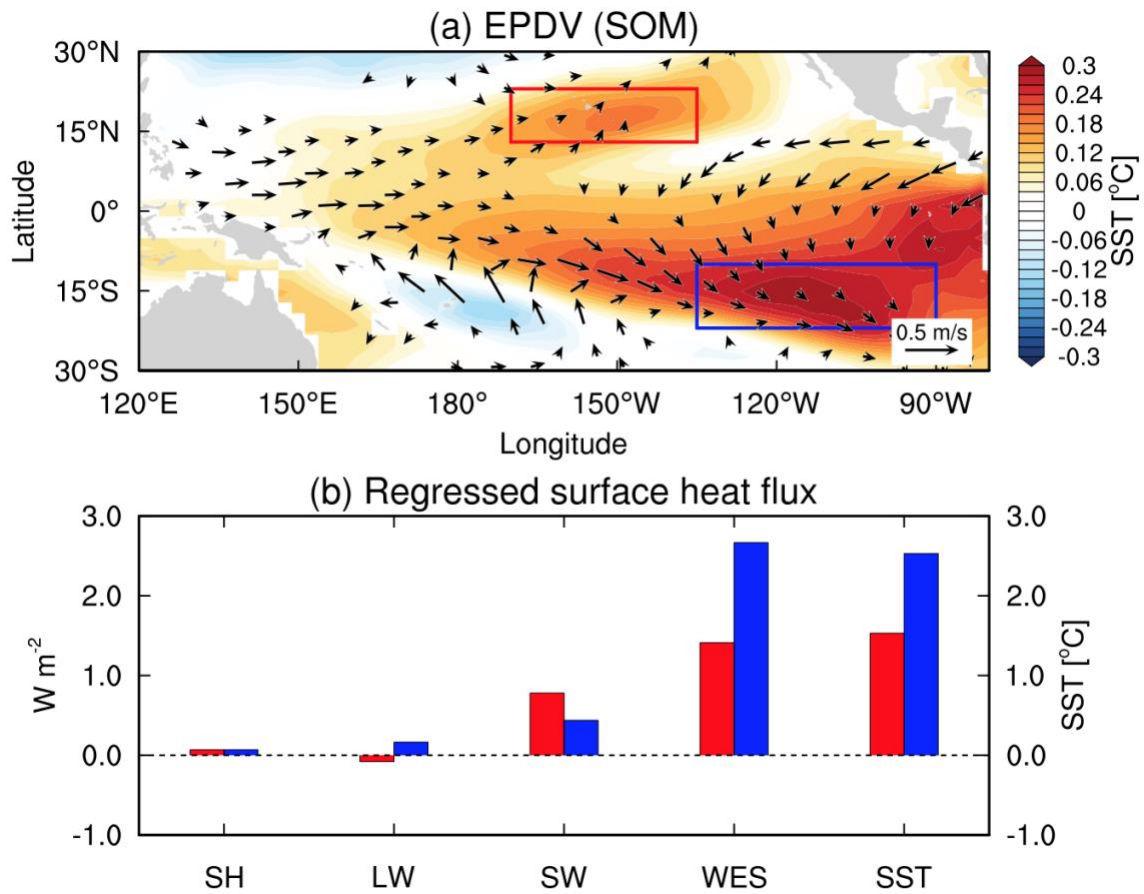


Figure S2. Equatorial asymmetry of EPDV-related SSTAs in the SOM. (a) Regressed tropical Pacific SSTAs (°C) and surface wind anomalies ($m s^{-1}$) against normalized EPDV PC. Red and blue boxes represent the locations of maximum SSTAs off the equatorial Pacific, respectively. (b) Regressed surface heat flux anomaly ($W m^{-2}$) against normalized 20-year low-pass filtered SSTAs averaged in the red (red bars) and blue (blue bars) boxes. SH: sensible heat; LW: longwave; SW: shortwave; WES: WES feedback, calculated by $-\overline{Q_E W'} / \overline{W}$, where Q_E is latent heat flux and W is wind speed (overbar denotes climatology and prime denotes anomaly departure from the climatology). The magnitudes of the 20-year low-pass filtered SSTAs averaged in the two boxes are plotted for comparison.

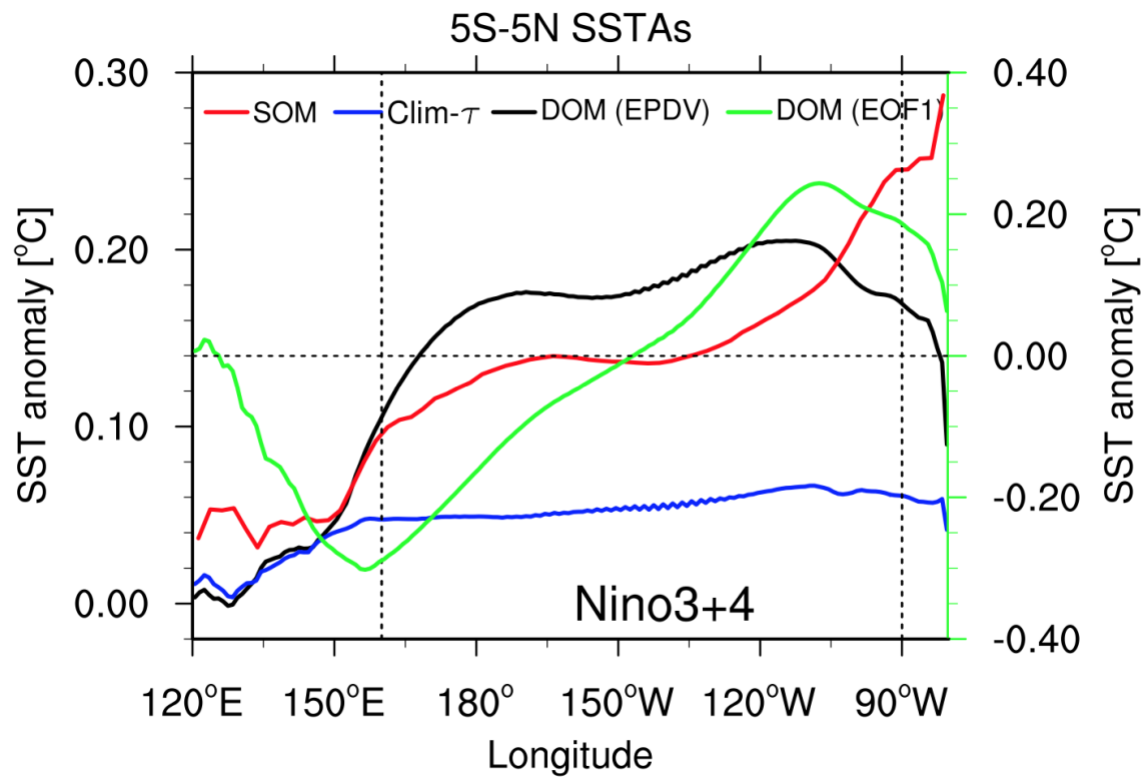


Figure S3. 5°S-5°N meridional mean of EPDV in Fig. 1 and DOM EOF1 in Fig. S1a (green line). Vertical dashed lines denote the longitudinal range of the Niño-3 plus Niño-4 region.

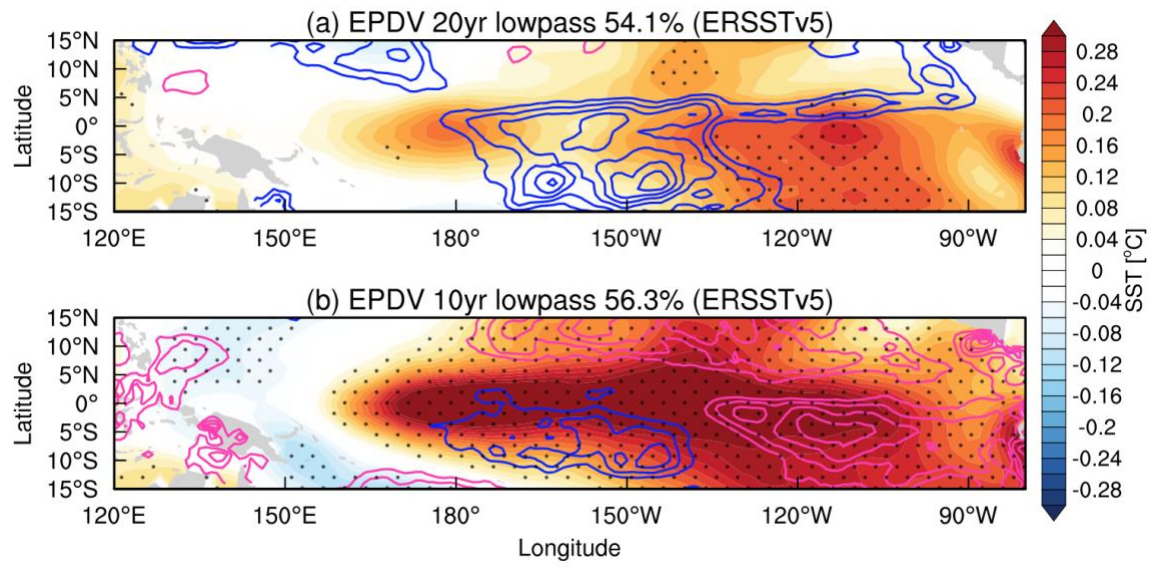


Figure S4. As in Fig. 4, but based on the ERSSTv5.